Effect of Calcination Temperature on the Stability of the Perovskite Materials – Study of Structural and Morphological Properties

Amina Maou[1*], Najwa Gouitaa[1], Taj Dine Lamcharfi[1], Noureddine Idrissi Kandri[1]

[1] Signals, Systems and Components Laboratory (LSSC), University Sidi Mohamed Ben Abdellah USMBA, FST, Fez, Immouzer Road B.P.2202, Morocco

[*] Corresponding author's e-mail: amina.maou@usmba.ac.ma

ABSTRACT

In this research, the solid-state method was utilized to synthesize $LaFeO_3$ powders, with La_2O_3 and Fe_2O_3 being employed as precursor materials. The prepared samples were calcined at different temperatures 800°C, 900°C, 1000°C, 1100°C, 1200°C and 1300°C for 4h to study phase stability. The thermal effect on structural and morphological properties was reported. The X-ray diffraction results confirmed the pure phase in its orthorhombic configuration at 1200°C and 1300°C, which was confirmed by Rietveld's analysis. Scanning electron microscopy coupled with Energy-dispersive X-ray spectroscopy was employed to analyze the surface morphology and compositional characteristics. In addition, the samples were analyzed by Fourier Transform Infrared Spectroscopy. The thermal behavior of the product was investigated through the utilization of thermogravimetric analysis.

Keywords: $LaFeO_3$, perovskites, solid-state, X-ray diffraction, infrared spectroscopy, thermogravimetric analysis.

INTRODUCTION

The ABO3 perovskites are crystalline and stable materials. They exhibit the flexibility to fabricate novel materials with enhanced material properties, based on large-size rare earth or alkaline earth metal at A-site, while transition metal at B-site. Thus, the properties of these types of material will be improved by the substitution or doping of new elements at different sites (Saumitra et al. 2012; Toan et al. 2003). Perovskites are materials characterized by several properties (structural, dielectric, electrical, optical, magnetic, and photocatalytic, etc.) which have attracted the attention of many researchers over the last few years to use them in several applications: as a catalyst, sensor materials, cathode material in solid oxide fuel cells, sewage treatment, and gas-sensitive materials (Sun et al. 2011; Mahapatra et al. 2018). In practice, the rare-earth orthoferrites $RFeO_3$ (R = rare earth element) have an orthorhombic symmetry with a Pbnm space group. Lanthanum ferrite oxide $LaFeO_3$ (LFO) is the most studied one of

these materials (Gao et al. 2019; Lee et al. 2021). Consequently, the Nèel temperature (TN=740 K) of LFO is the highest in the ferrite system (Qing Lin et al. 2018). Due to its advantageous features, such as a unique crystal structure, distinctive electromagnetic behavior, high electron/ion conductivity, excellent catalytic activity, suitable thermal expansion coefficient, and chemical stability, this perovskite material finds extensive use in various industrial applications (Qing Lin et al. 2018). LFO has been prepared using various methods, including co-precipitation (Kumar et al. 2009; Nakayama 2001), sol-gel (Ismael and Wark 2019; Qing Lin et al. 2018), hydrothermal (Mesbah et al. 2020; Jairo et al. 2016; Wenjun Zheng et al. 2000), the polymerized complex method (Phokha et al. 2014), combustion method (Priti et al. 2010; Komova et al. 2016), and solid-state method (Qiang Li et al. 2021; Sazelee et al. 2019). Most researchers on this perovskite are interested in the catalytic, photocatalytic, dielectric, and magnetic properties; Kucharczyk et al. reported that the physicochemical properties of LFO perovskite

and its methane oxidation activity depend on the preparation conditions (temperature and calcination time) and they found that when the calcination temperature increases the BET-specific surface area of perovskite decreases (Kucharczyk et al. 2019). Saumitra et al. synthesized LFO by using the sol-gel method and they studied the photocatalytic water splitting reaction for hydrogen generation under visible light irradiation, showing noticeable hydrogen enhancement using ethanol as a sacrificial donor and Platine as cocatalyst (Saumitra et al. 2012). Lee et al. (2021) reported the colossal dielectric response, multiferroic properties, and gas-sensing characteristics of the rare earth orthoferrite LFO ceramics. All these works have not discussed the thermal effect of calcination on the properties structural and morphologic for LFO. For this reason, this article focused on the synthesized $LaFeO_3$ powders by using a solid-state method and calcined at different temperatures, i.e. 800°C, 900°C, 1000°C, 1100°C, 1200°C and 1300°C for 4 h for the study of stability phase of LFO. The powders were subjected to characterization using X-ray diffraction (XRD), Fourier transform infrared (FTIR), scanning electron microscopy (SEM) combined with energy-dispersive X-ray spectroscopy (EDS), and thermogravimetric analysis (TGA). These techniques were employed to investigate the impact on the structural and morphological properties of the samples.

EXPERIMENT

Samples preparation:

The $LaFeO_3$ powders were elaborated by the solid-state reaction using lanthanum oxide La_2O_3 and iron oxide Fe_2O_3 with high purity (99.99%) starting materials. These precursors were mixed in a stoichiometric amount according to the following reaction:

$$½ La_2O_3 + ½ Fe_2O_3 \rightarrow LaFeO_3 \qquad (1)$$
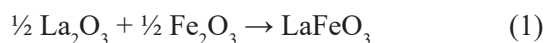
The precursor materials were initially mixed for 0.5 hours and subsequently homogenized by milling in the presence of acetone for a total of 4 hours. Following this step, the resulting powders were dried at a temperature of 100°C for a period of 24 hours. Finally, the dried powders were further mixed using an agate mortar for 30

minutes. The powder mixture was transferred into an alumina crucible and subjected to calcination in an air environment at various temperatures, namely 800°C, 900°C, 1000°C, 1100°C, 1200°C, and 1300°C. The calcination process was carried out in a Nabertherm furnace, under a static air atmosphere, with a heating rate of 3°C per minute. Following the calcination, all specimens were allowed to cool down to room temperature in ambient air. A visual representation of the different steps involved in the preparation method of $LaFeO_3$ is depicted in Figure 1.

Characterization

X-ray diffraction analysis: the LFO powders were characterized by X-ray diffraction measurement using a Panalytical X'Pert Pro X-ray diffractometer equipped with a Cu-Kα monochromatic source (λ = 1,54056 Å). For scanning electron microscopy coupled to EDS, the morphology and microstructure were made by using a scanning microscope (Jeol it500 HR). The samples were analyzed using a Bruker vortex 70 FTIR spectrometer resting on ATR mode. The registering of FTIR spectra for a wavelength ranged from 400 to 4000 cm^{-1}. For the thermogravimetric analysis, recorded the mass loss between 25°C and 1250°C at a heating rate of 3°C/min using a simultaneous thermobalance (TG+DSC) with a LINSEIS high range type (LINSEIS STA PT 1600).

RESULTS AND DISCUSSION

X-ray diffraction

Figure 2 shows the XRD patterns of the synthesized LFO samples calcined at different temperatures for 4 hours. All diffractograms for these ceramics were acquired under the same operating conditions. For calcination temperatures lower than 1100°C, crystallization of the phase in its Orthorhombic (Pbnm space group) configuration was observed with the presence of various secondary phases associated with La_2O_3 and Fe_2O_3 (starting precursor). Beyond this temperature, the structure remains stable and the intensity of the secondary peaks decreased until its complete disappearance at the temperature of 1200°C. From the literature, it was found that the calcination temperature of LFO material is not fixed. According to previous works which
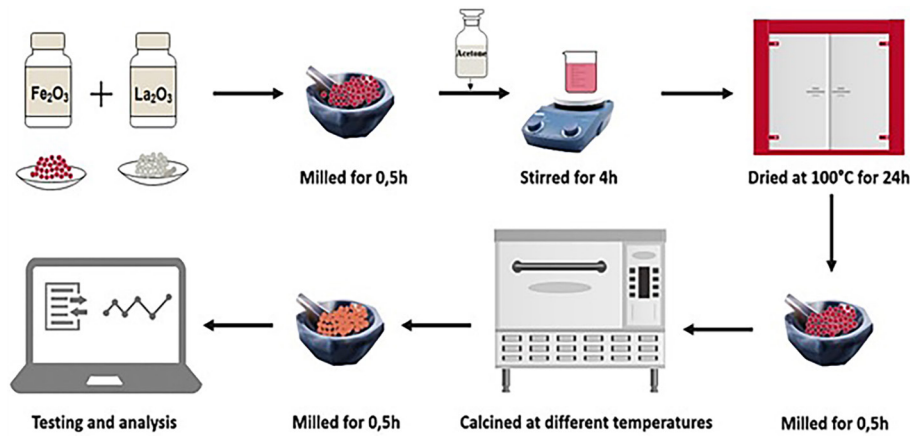
Fig. 1. Systematic synthesis procedure for LFO powders

prepared this material with the same method as the one used in this paper (solid state method), this temperature varies between 1000 for 24 and 1500°C as shown in Table 1. All of these studies confirm the orthorhombic phase of LFO with different space groups. Considering this, it was decided to subject the compound to various calcination temperatures to examine both its behavior and phase stability.

Rietveld refinement

For more information on the structure and to confirm the results obtained in the X-ray diffraction, the Rietveld refinement was studied using the Fullprof software. The peak pattern was carried out using a pseudo-Voigt function. In detail, the background level was described by a polynomial function with 12 coefficients. The Rietveld refinement of the studied samples calcined at 1100°C, 1200°C and 1300°C was presented in Figure 3. In the visual representation, the experimental data is depicted by the red color, while the black line in red color represents the Rietveld refinement. Additionally, the blue line represents the difference between the experimental data and the Rietveld refinement. The obtained refinement results
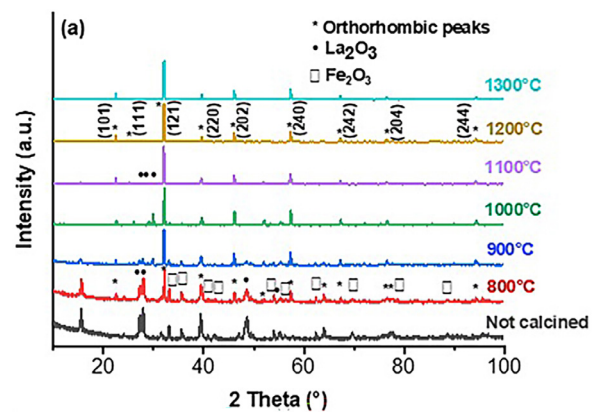

Fig. 2. X-ray diffraction patterns of LFO powders obtained at different calcination temperatures for a duration of 4 hours

provide confirmation of the presence of three distinct phases: $LaFeO_3$ (orthorhombic phase with Pbnm space group), Fe_2O_3, and La_2O_3. In addition, this result confirms the pure phase at 1200°C (i.e. no peaks indicating the existence of secondary phases of La_2O_3 and Fe_2O_3). The Rietveld refinement was allowed to plot by the software VESTA the crystal structure of LFO calcined at 1200°C was presented in Figure 3, this structure shows that site A is La and site B is occupied by Fe, and (O_1, O_2) the different oxygen sites. La^{3+}

Table 1. Comparison of the thermal treatment, crystal system/space group, of the LFO powder synthesis by solid-state method with previous works

No.	Crystal system/space group	Thermal treatment	Reference
1	Orthorhombic/Pbnm	Calcined at 1400 °C/4h	[21]
2	Orthorhombic/Pbnm	Preheated at 1000 °C/2h Calcined at 1200 °C/4h	[5]
3	Orthorhombic/Pnma	1500 °C/6h	[22]
4	Orthorhombic/Pnma	La_2O_3 calcined at 900 °C/12h $LaFeO_3$ calcined at 1000 °C/24h	[23]
5	Orthorhombic/Pbnm	1200 °C/4h	This work
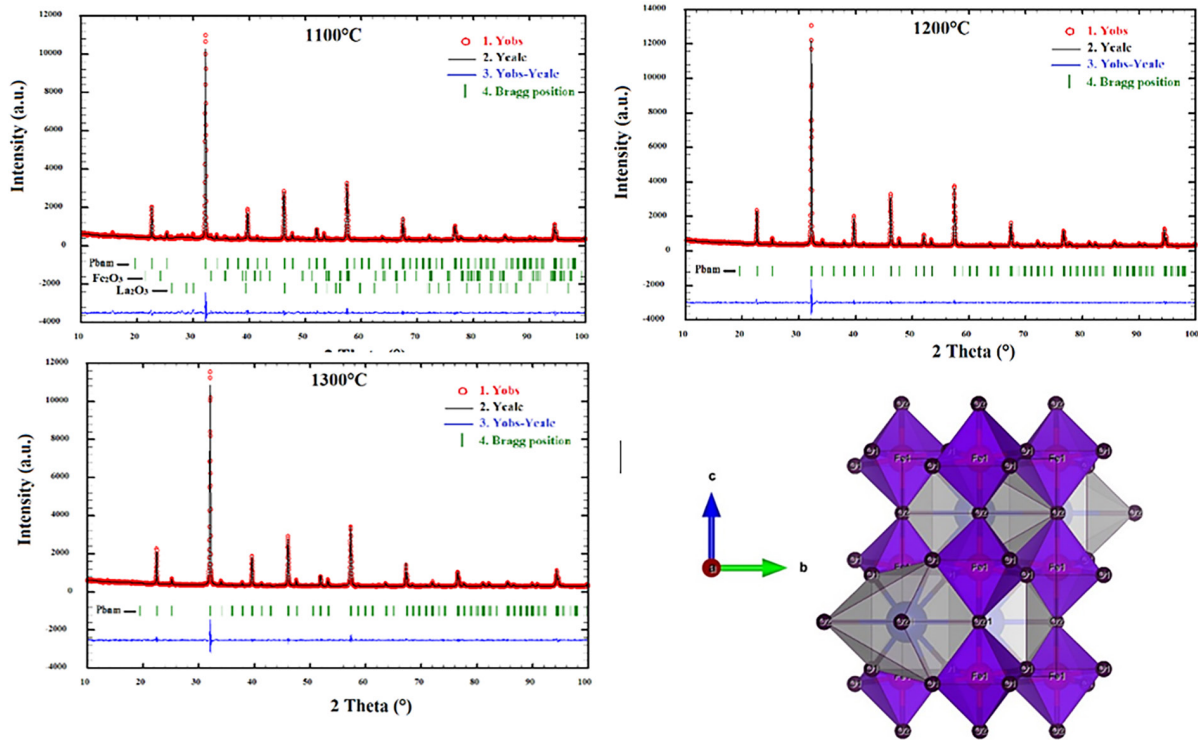
Fig. 3. Rietveld refinement for LFO calcined at 1100°C, 1200°C and 1300°C 4 h and the representation of polyhedral LFO calcined at 1200°C/4h obtained by the VESTA software

is attached to eight O^{2-} atoms in eight-coordinate geometry and Fe^{3+} is related to six O^{2-} atoms to form FeO_6 octahedra with divided corners.

Table 2 displays the lattice parameters (a, b, c), unit cell volume (V), and Rietveld refinement Σ^2 values for the LFO material calcined at different temperatures (1100°C, 1200°C, and 1300°C). From this table, it can be seen that with increasing temperature, the value of the quality of fit Σ^2 decrease which indicates good crystallinity of the phase with a small change in lattice parameters which that confirmed the stability of the phase. The average grain size of this sample was calculated by the Debye-Scherrer equation (Ismael and Wark 2019; Qing Lin et al. 2018):

$$D = \frac{K\lambda}{\beta cos\theta} \qquad (2)$$

At a calcination temperature of 1200°C, the average grain size (D) of the LFO material was determined to be 95.63 nm. The calculation of D involves the parameters: K (crystallite shape factor), λ (copper wavelength, λ = 0.15405 nm), θ (Bragg diffraction angle), and β (full width at half maximum FWHM) obtained from the Rietveld refinement in the output file.

Infrared spectroscopy

Figure 4 shows the infrared spectrum of calcined LFO powders at different temperatures in the region 400–4000 cm^{-1}. The spectra exhibit two main bands, with the first band observed at 533 cm^{-1} attributed to the Fe-O stretching vibration. The second band, centered around 474 cm^{-1}, is likely associated with the O-Fe-O deformation vibration (Priti V et al. 2010). In addition, the presence of some bands can be observed for

Table 2. Lattice parameters (a, b, c), Unit cell V, and Σ2 at 1100°C, 1200°C and 1300°C for 4 hours

Temperature °C	Lattice constant			V(Å)	Σ²
	a (Å)	b (Å)	c (Å)		
1100	5.5498	5.5614	7.8474	242.2032	1.704
1200	5.5503	5.5622	7.8483	242.2917	1.13
1300	5.5496	5.5612	7.8468	242.1709	1.13

temperature lower than 1000°C, one at 3610 cm^{-1} which is related to the vibration of the OH group according to the work reported in the literature (Lin et al. 2018; Li et al. 2007; Bhat et al. 2013; Khalil et al. 2022). The presence of two bands in the range of 1380 to 1490 cm^{-1} can be attributed to the asymmetric stretching vibration of metal carbonates, specifically corresponding to the C-H and C-C bonds (Lin et al. 2018; Khalil et al. 2022; Feng et al. 2011; Tang et al. 2013), respectively. For the other temperatures and above two bands related to the LFO material (Fe-O, O-Fe-O) the disappearance of the OH, C-H, and C-C bands and the appearance of two new bands in the range between 1990 and 2110 cm^{-1} were noted. These two bands are corresponding to the specific C=O double bond vibration of carbon dioxide CO_2 according to Vijayaraghavan et al. (2017). On the other hand, with the increase in calcination temperature, the intensity of the bands related to carbon bonds and OH bonds gradually decreases, which is probably related to small amounts of acetone residues. These bonds are not detected by XRD and are observed in Infrared analysis and formed mainly at the surface due to exposure to ambient air (Feng et al. 2011). Also, there is the appearance of CO_2 which can be related to their release on the surface of the powders.

Scanning electron microscopy analysis

Scanning electron microscopy is an imaging technique that utilizes electrons instead of light to generate high-resolution images. It enables the examination of the microscopic surface structure of materials by scanning their surfaces (Humera Sabeeh et al. 2018). This analysis has been performed to probe the morphology and grain size. Figure 5 presents the SEM images and the results of the grain size analysis of LFO powders calcined at 1100°C, 1200°C and 1300°C for 4 h. It was observed that the majority of the particles are homogeneously distributed and the grain size is not uniform and has a semi-spherical morphology. From these SEM images, the average particle size was calculated by fitting the particle size distribution histogram using ImageJ software. It was found that the average particle size is 820 nm, 1077 nm, and 1312 nm for 1100°C, 1200°C, and 1300°C respectively, which means that the particle size increases by increasing the calcination temperature. Therefore, it can be concluded that the calcination temperature significantly modifies the surface morphology.
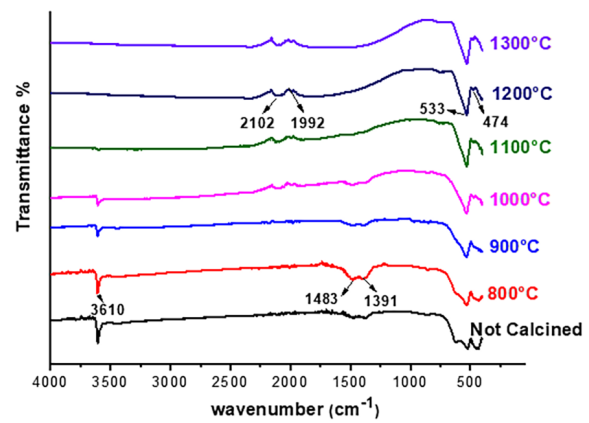

Fig. 4. FTIR spectra of the LFO samples at different calcination temperatures

Energy-dispersive X-ray spectroscopy analysis

Figure 6 shows the energy-dispersive X-ray spectroscopy LFO material calcined at 1100°C, 1200°C, and 1300°C. SEM is a valuable technique employed to investigate the purity and chemical composition of the synthesized particles, providing qualitative insights into the sample composition. Analysis of Figure 6 and Table 3 reveals the presence of all essential elements of $LaFeO_3$, including lanthanum (La), iron (Fe), oxygen (O), and carbon (C). The detection of carbon, associated with the coating material on the sample, further confirms the findings obtained from the Infrared-spectrum analysis (Fig. 4).

Thermogravimetric analysis

To confirm the calcination temperature appropriate for the formation of a crystalline phase. The synthesized sample was characterized by thermogravimetric analysis. Figure 7 indicates the thermal analysis of the LFO particles. The result was registered in a temperature range of 25°C up to 1200°C with a heating rate of 3 degrees/min. It was found that a total mass loss of 10% in this temperature range is divided into three-step; two steps of weight loss and one-step of mass gain; the first is a loss of 4.61% occurs around 312°C up to 359.83°C which it was attributed to the evaporation of volatile organic substances. The second step is a gain of mass of 2.92% at 350°C to 460°C that is probably related to the fixation of a gas. The final step is a loss of 7.46% around 712.66°C up to 850°C; this may be due to the degassing of adsorbed elements. Furthermore, above 850°C, there is no loss of mass indicating the absence of organic matter, and residual
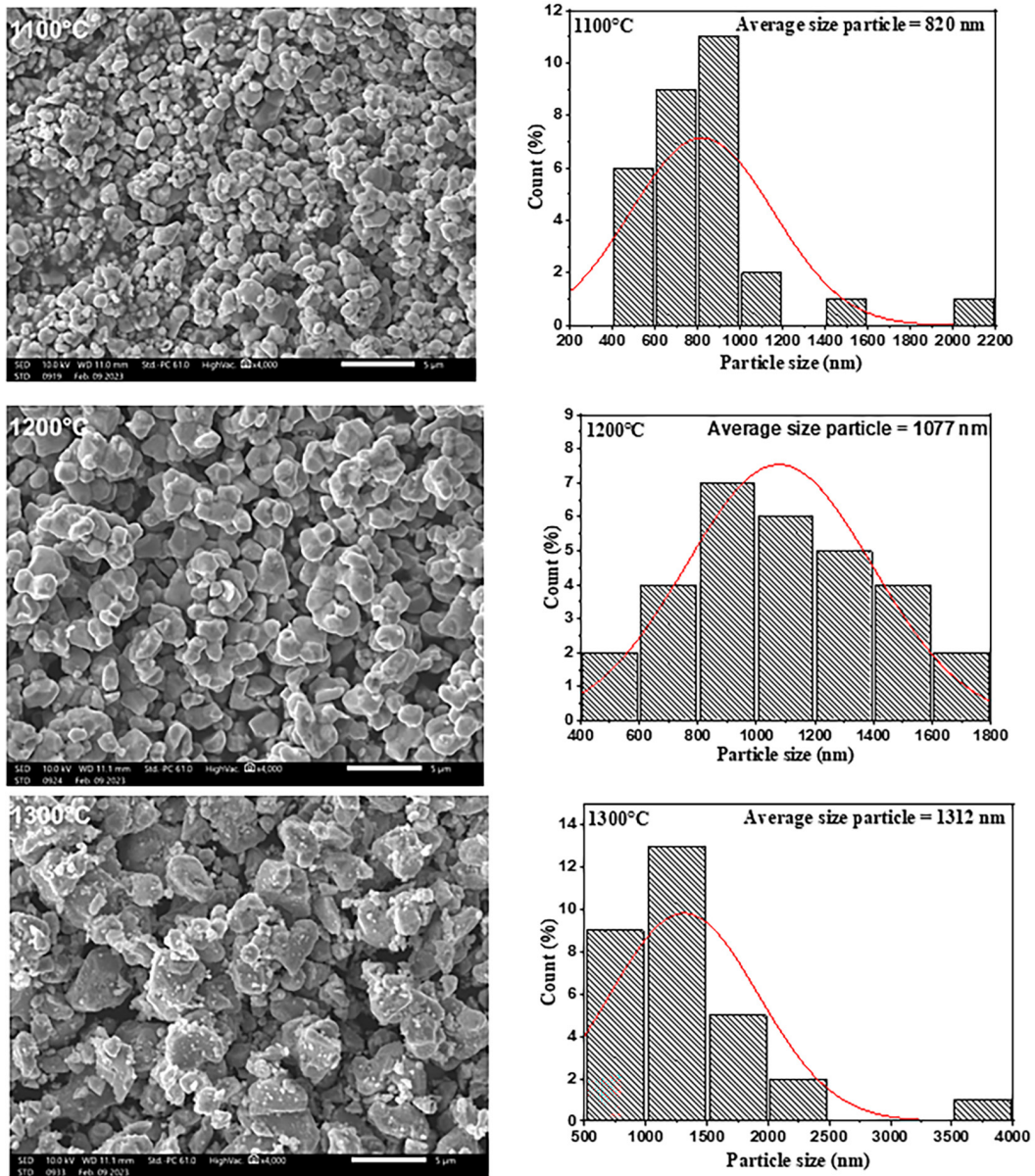
Fig. 5. SEM of the surface of LFO samples calcined at 1100°C, 1200°C, and 1300°C associated particle size distributions
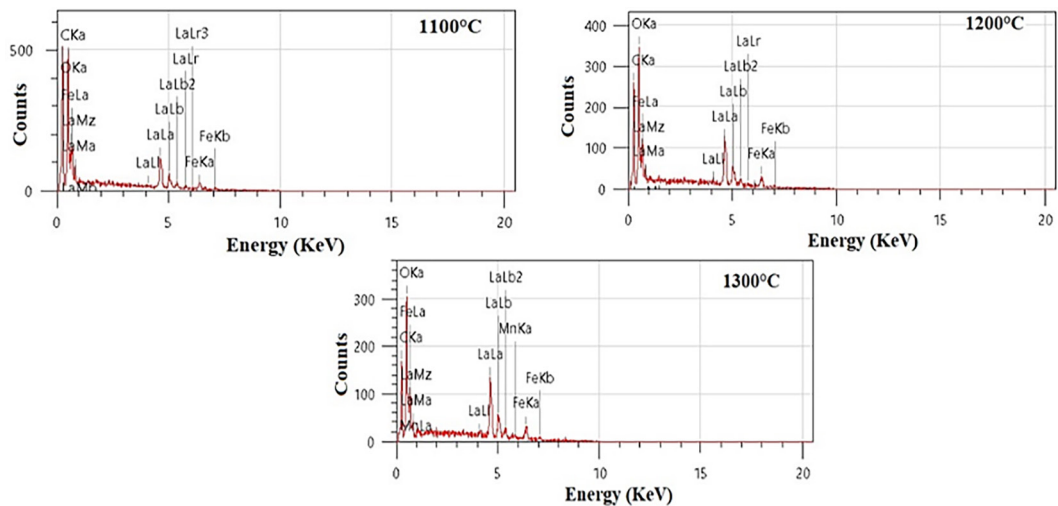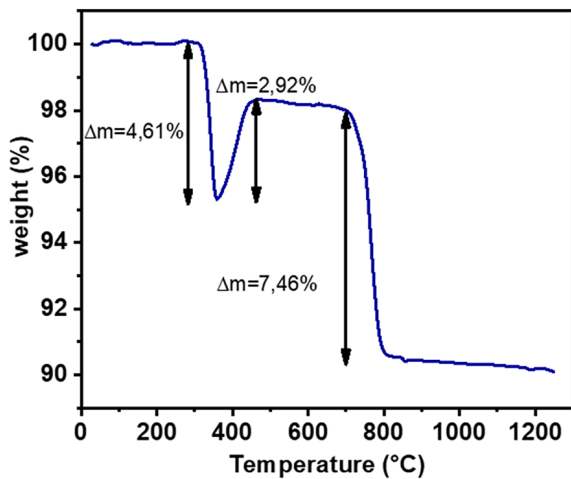

Fig. 6. Results of EDS analysis of LFO powders calcined at 1100°C, 1200°C and 1300°C for 4h

Table 3. EDS data of LFO calcined at 1100°C, 1200°C and 1300°C for 4h

Element	Content (%)		
	1100 °C	1200 °C	1300 °C
C	22.01	26.73	23.04
O	43.72	40.68	40.43
Fe	14.90	14.65	16.12
La	19.36	17.94	20.40

Fig. 7. Thermogravimetric analysis of LFO

reagents, which suggests the formation of the stable phase of LFO. The observations align with the findings from the X-ray diffraction patterns of LFO samples calcined at various temperatures, affirming the transition of the amorphous phase to the crystalline phase starting from 800°C.

CONCLUSIONS

In conclusion, the synthesis of LFO using the solid-state method was successfully achieved. The impact of varying calcination temperatures on the structural, microstructural, and morphological properties has been thoroughly discussed. The X-ray diffraction results, analyzed using the Rietveld refinement method, indicate that at temperatures starting from 1200°C, the LFO structure is pure, with no secondary phases present. This finding demonstrates the stability of the LFO phase at higher temperatures. Infrared analysis indicates the coexistence of the two principal bands Fe-O and Fe-O-Fe for all calcination temperatures. SEM images present a homogeneous semi-spherical structure and the average particle size rises with increasing calcination temperature. EDS results demonstrate the presence of elements

composed of LFO (La, Fe, and O). The ATG analysis shows the calcination temperature adequate for LFO to be pure. On the basis of the extensive analyses conducted, it can be concluded that the optimal calcination temperature for achieving LaFeO$_3$ is 1200°C. Furthermore, the phase stability of LaFeO$_3$ is observed up to 1300°C.

REFERENCES

1. Mahapatra A.S., Mitra A., Mallick A., Shaw A., Greneche J.M., Chakrabarti P.K. 2018. Modulation of magnetic and dielectric property of LaFeO$_3$ by simultaneous doping with Ca^{2+} and Co^{2+}-ions. Journal of Alloys and Compounds, 2.

2. Mahapatra A.S., Mitra A., Mallick A., Ghosh M., Chakrabarti P.K. 2016. Enhanced magnetic property and phase transition in Ho^{3+} doped LaFeO$_3$. Materials Letters. S0167–577X(16)30117–3

3. Kucharczyk B., Okal J., Tylus W., Winiarski J., Szczygieł B. 2019. The effect of the calcination temperature of LaFeO$_3$ precursors on the properties and catalytic activity of perovskite in methane oxidation. Ceramics International.

4. Sabeeh H., S. Musaddiq, M. Shahid, M.A. Khan, M. Sher, M. Farooq Warsi. 2018. Rare Earth Substituted Nanocrystalline LaFeO3 Perovskites and their Composites with Reduced Graphene Oxide for Enhanced Photocatalytic and other Potential Applications. Materials Research Express.

5. Bhat I., S. Husain, W. Khan, S.I. Patil. 2013. Effect of Zn doping on structural, magnetic and dielectric properties of LaFeO$_3$ synthesized through sol–gel auto-combustion process. Materials Research Bulletin.

6. Jiansheng Feng, Ting Liu, Yebin Xu, Jingyuan Zhao, Yanyan He. 2011. Effects of PVA content on the synthesis of LaFeO$_3$ via sol–gel route. Ceramics International.

7. Gomez-Cuaspud J.A., E. Vera-Lopez, J.B. Carda-Castello, E. Barrachina-Albert. 2016. One-step hydrothermal synthesis of LaFeO$_3$ perovskite for methane steam reforming. Reac Kinet Mech Cat.

8. Kamal M.S. Khalil, Abdelrahman H. Mahmoud,

Mohamed Khairy. 2022. Formation and textural characterization of size-controlled LaFeO$_3$ perovskite nanoparticles for efficient photocatalytic degradation of organic pollutants. Advanced Powder Technology.

9. Lee K., S. Hajra, M. Sahu, H.J. Kim. 2021. Colossal dielectric response, multiferroic properties, and gas sensing characteristics of the rare earth orthoferrite LaFeO$_3$ ceramics. Journal of Alloys and Compounds.

10. Lihui Sun, Hongwei Qin, Kaiying Wang, Ming Zhao, Jifan Hu. 2011. Structure and electrical properties of nanocrystalline La1−xBaxFeO3 for gas sensing application. Materials Chemistry and Physics.

11. Kumar M., Srikanth S., Ravikumar B., Alex T.C., Das S.K. 2009. Synthesis of pure and Sr-doped LaGaO$_3$, LaFeO$_3$ and LaCoO$_3$ and Sr,Mg-doped LaGaO$_3$ for ITSOFC application using different wet chemical routes. Materials Chemistry and Physics.

12. Mohammed Ismael, Michael Wark. 2019. Perovskite-type LaFeO3: Photoelectrochemical Properties and Photocatalytic Degradation of Organic Pollutants Under Visible Light Irradiation. Catalysts.

13. Mesbah M., S. Hamedshahraki, S. Ahmadi, M. Sharifi, C.A. Igwegbe. 2020. Hydrothermal synthesis of LaFeO$_3$ nanoparticles adsorbent: Characterization and application of error functions for adsorption of fluoride. MethodsX.

14. Toan N.N., Saukko S., Lantto V. 2003. Gas sensing with semiconducting perovskite oxide LaFeO3. Physica B.

15. Sazelee N.A., Yahya M.S., Idris N.H., Md Din M.F., Ismail M. 2019. Desorption properties of LiAlH4 doped with LaFeO$_3$ catalyst. international journal of hydrogen energy

16. Sivakumar N., J.Gajendiran, AliAlsalme, KentaroTashiro. 2022. Structural, morphological, optical, magnetic and electrochemical behavior of solid-state synthesized pure and Sr-doped LaFeO3 nanoparticles. Physica B: Condensed Matter.

17. Komova O.V., Simagina V.I., Mukha S.A., Netskina O.V., Odegova G.V., Bulavchenko O.A., Ishchenko A.V., Pochtar A.A. 2016. A modified glycine–nitrate combustion method for one-step synthesis of LaFeO3. Advanced Powder Technology.

18. Priti V. Gosavi, Rajesh B. Biniwale. 2010. Pure phase LaFeO3 perovskite with improved surface area synthesized using different routes and its characterization. Materials Chemistry and Physics

19. Peisong Tang, Yi Tong, Haifeng Chen, Feng Cao, Guoxiang Pan. 2013. Microwave-assisted synthesis of nanoparticulate perovskite LaFeO$_3$ as a high active visible-light photocatalyst. Current Applied Physics.

20. Qing Lin, Jinpei Lin, Xingxing Yang, Yun He, Liping Wang, Jianghui Do. 2018. The effects of Mg2+ and Ba2+ dopants on the microstructure and magnetic properties of doubly doped LaFeO$_3$ perovskite catalytic nanocrystals. Ceramics International.

21. Qing Lin, Xingxing Yang, Jinpei Lin, Zeping Guo, Yun He. 2018. The structure and magnetic properties of magnesium-substituted LaFeO$_3$ perovskite negative electrode material by citrate sol-gel. International journal of hydrogen energy.

22. Qiang Li, Guangzhou Zhu. 2021. Controlling negative permittivity and permeability behavior in LaFeO3 through sintering temperature. Ceramics International.

23. Qing Lin, Jianmei Xu, Fang Yang, Xingxing Yang and Yun He. 2018 The influence of Ca substitution on LaFeO$_3$ nanoparticles in terms of structural and magnetic properties. Journal of Applied Biomaterials & Functional Materials.

24. Saumitra N. Tijare, Meenal V. Joshi, Priyanka S. Padole, Priti A. Mangrulkar, Sadhana S. Rayalu, Nitin Labhsetwar K. 2012. Photocatalytic hydrogen generation through water splitting on nano-crystalline LaFeO3 perovskite. International Journal of Hydrogen Energy.

25. Acharya S., J. Mondal, S. Ghosh, S.K. Roy, P.K. 2010. Chakrabarti. Multiferroic behavior of lanthanum orthoferrite (LaFeO$_3$). Materials Letters.

26. Nakayama S. 2001. LaFeO3 perovskite-type oxide prepared by oxide-mixing, co-precipitation and complex synthesis methods. Journal of Materials Science.

27. Shudan Li, Liqiang Jing, Wei Fu, Libin Yang, Baifu Xin, Honggang Fu. 2007. Photoinduced charge property of nanosized perovskite-type LaFeO$_3$ and its relationships with photocatalytic activity under visible irradiation. Materials Research Bulletin.

28. Phokha S., S. Pinitsoontorn, S. Maensiri, S. Rujirawat. 2014. Structure, optical and magnetic properties of LaFeO$_3$ nanoparticles prepared by polymerized complex method. J Sol-Gel Sci Technol.

29. Vijayaraghavan T., Sivasubramanian R., Hussain S., and Ashok A. 2017. A Facile Synthesis of LaFeO3-Based Perovskites and Their Application towards Sensing of Neurotransmitters. ChemistrySelect.

30. Ting Ting Gao, Xiao Na Zhu, Jing Chen, Xiao Qiang Liu, Xiang Ming Chen, 2019. Conductive, dielectric, and magnetic properties of Y-substituted LaFeO$_3$ ceramics. Journal of Alloys and Compounds

31. Wenjun Zheng, Ronghou Liu, Dingkun Peng, Guangyao Meng, 2000. Hydrothermal synthesis of LaFeO$_3$ under carbonate-containing medium. Materials Letters.